Supplemental Digital Content

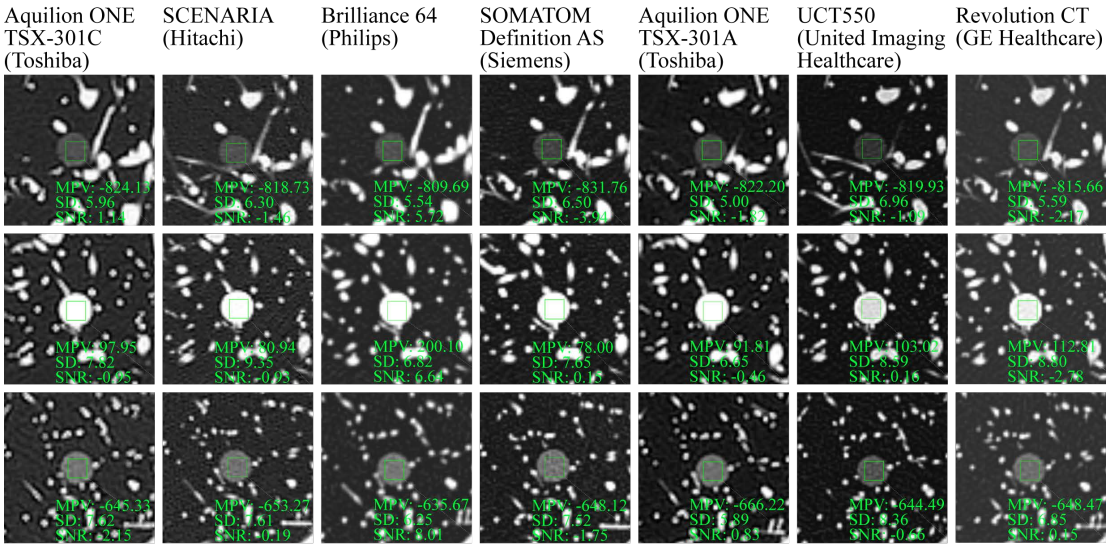

Figure S1: The CT images of three simulated nodules (diameter: 10 mm; CT attenuation values: -800, 100, and -630 Hounsfield units from the top to the bottom) with their internal square segmentations in the inter-CT trial. MPV = mean pixel values. SD = standard deviation. SNR = signal-to-noise ratio.

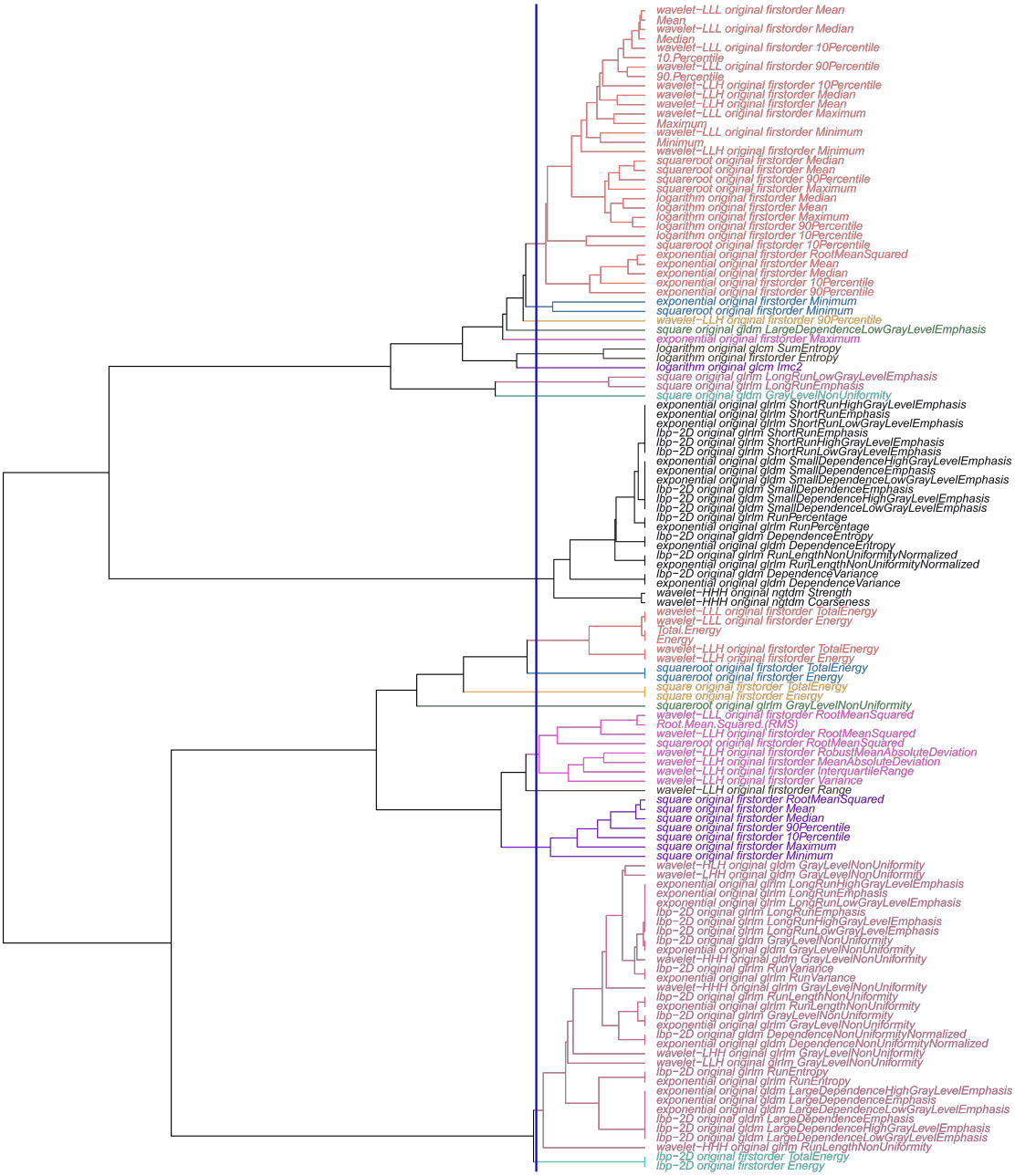

Figure S2: The dendrogram shows hierarchical clustering of the total intersection of 124 RFs.

The blue line was chosen to differentiate 19 separated clusters. RF = radiomic feature.

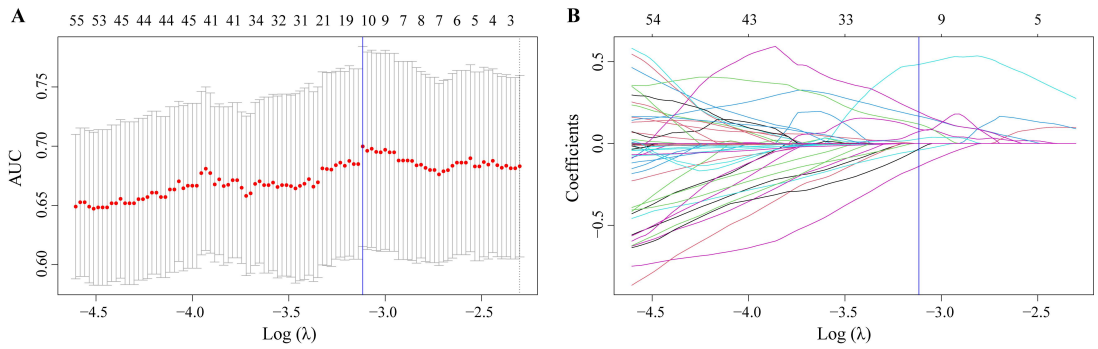

Figure S3: (A) RF selection with the LASSO regression model according to the AUC value. The blue vertical line was drawn at the optimal λ value based on the minimum criteria and 1 standard error of the minimum criteria. (B) LASSO coefficient profiles of the 1171 RFs. The blue vertical line was drawn at the optimal λ, which resulted in 10 non-zero coefficients. RF = radiomic feature. LASSO = least absolute shrinkage and selection operator. AUC = area under curve.

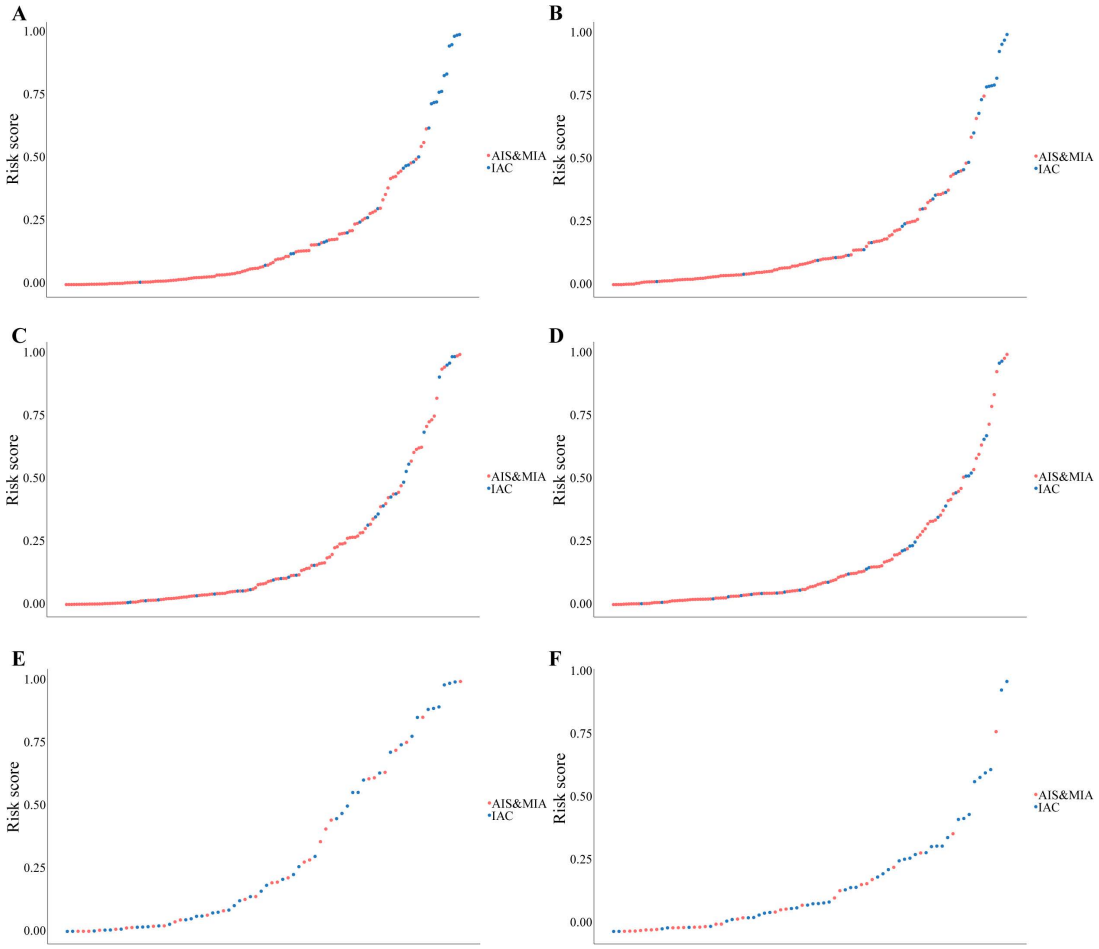

Figure S4: The predicted risk score of the "unstable model" in the training dataset (A), testing dataset (C), and validation dataset (E). The predicted risk score of the "stable model" in the training dataset (B), testing dataset (D), and validation dataset (F). The color of the sample point corresponds to the true pathological diagnosis. The larger the predicted risk score of a sample point, the more likely will it be predicted as an IAC. AIS = adenocarcinoma in situ. MIA = minimally invasive adenocarcinoma. IAC = invasive adenocarcinoma.

Table S1: Characteristics of the Clinical Dataset

	Training Dataset	Testing Dataset	Validation Dataset	Total Dataset
No. of patients [a]	146	150	70	353
No. of lesions	155	155	74	384
CTDI (mGy) [b]	10.35 (1.10–33.40)	9.58 (1.21–33.40)	5.83 (2.26–14.07)	8.84 (1.10–33.40)
Age (years) [c]	51.42 ± 11.62	50.69 ± 10.98	52.19 ± 11.83	51.18 ± 11.40
Gender				
Male	40/146 (27.40%)	37/150 (24.67%)	12/70 (17.14%)	87/353 (24.65%)
Female	106/146 (72.60%)	113/150 (75.33%)	58/70 (82.86%)	266/353 (75.35%)
Pathological diagnosis				
AIS and MIA	126/155 (81.29%)	126/155 (81.29%)	30/74 (40.54%)	282/384 (73.4%)
IAC	29/155 (18.71%)	29/155 (18.71%)	44/74 (59.46%)	102/384 (26.6%)
Type of nodule				
PGGN	112/155 (72.26%)	107/155 (69.03%)	40/74 (54.05%)	259/384 (67.4%)
MGGN	43/155 (27.74%)	48/155 (30.97%)	34/74 (45.95%)	125/384 (32.6%)
Spiculation				
No	65/155 (41.94%)	69/155 (44.52%)	59/74 (79.73%)	193/384 (50.3%)
Yes	90/155 (58.06%)	86/155 (55.48%)	15/74 (20.27%)	191/384 (49.7%)
Lobulation				
No	49/155 (31.61%)	53/155 (34.19%)	39/74 (52.70%)	141/384 (36.7%)
Yes	106/155 (68.39%)	102/155 (65.81%)	35/74 (47.30%)	243/384 (63.3%)
Bubblelike appearance				
No	129/155 (83.23%)	127/155 (81.94%)	55/74 (74.32%)	311/384 (81.0%)
Yes	26/155 (16.77%)	28/155 (18.06%)	19/74 (25.68%)	73/384 (19.0%)
Tumor-lung interface (clear)				
No	27/155 (17.42%)	22/155 (14.19%)	40/74 (54.05%)	89/384 (23.2%)
Yes	128/155 (82.58%)	133/155 (85.81%)	34/74 (45.95%)	295/384 (76.8%)
Air bronchogram				
No	91/155 (58.71%)	101/155 (65.16%)	52/74 (70.27%)	244/384 (63.5%)
Yes	64/155 (41.29%)	54/155 (34.84%)	22/74 (29.73%)	140/384 (36.5%)
Pulmonary vascular change				
No	35/155 (22.58%)	37/155 (23.87%)	15/74 (20.27%)	87/384 (22.7%)
Yes	120/155 (77.42%)	118/155 (76.13%)	59/74 (79.73%)	297/384 (77.3%)
Pleural indentation				
No	119/155 (76.77%)	127/155 (81.94%)	55/74 (74.32%)	301/384 (78.4%)
Yes	36/155 (23.23%)	28/155 (18.06%)	19/74 (25.68%)	83/384 (21.6%)

Note.—CTDI = CT dose index. AIS = adenocarcinoma in situ. MIA = minimally invasive adenocarcinoma. IAC = invasive adenocarcinoma. PGGN = pure ground-glass nodule. MGGN = mixed ground-glass nodule.

[a] Since the randomization of the training and testing datasets was performed at the lesion level and divided the lesions of the same patient into different datasets, the number of some patients was double-counted so that the total patients' number of three datasets differed from the total number of patients.

[b] The average and range of CTDI were expressed as mean (min–max).

[c] Plus-minus values were mean ± SD.

Table S2: The CT Acquisition Parameters Used for the Clinical Dataset

CT Scanner (Manufacturer)	Collimation (mm) [a]	Tube Voltage (kVp)	Tube Current (mA) [b]	Rotation Time (s)	Slice Thickness (mm)	Lung Window Settings - Width (HU)	Lung Window Settings - Level (HU)	Mediastinal Window Settings - Width (HU)	Mediastinal Window Settings - Level (HU)	Pitch
Brilliance (Philips) [c]	64 × 0.625	120	150–200	0.75	1	1200	−600	400	40	0.906
Somatom Definition AS (Siemens Healthineers) [d]	128 × 0.6	120	150–200	0.5	1	1200	−600	400	40	1.2
Scenaria (Hitachi) [e]	64 × 0.625	120	150–200	0.5	1	1200	−600	400	40	0.906
Aquilion One (Toshiba) [f]	160 × 0.5	120	150–200	0.6	1	1200	−600	400	40	0.828

Note.—HU = Hounsfield units.

[a] Number of slices multiplied by thickness.

[b] Tube current was automatically adjusted within the range of 150-200 mA.

[c] Brilliance (Philips) contributed to 70 sets of CT images in the validation dataset.

[d] Somatom Definition AS (Siemens Healthineers) contributed to 56 sets of CT images in the training dataset and 59 in the testing dataset.

[e] Sixty-four channels and 128 slices. Scenaria (Hitachi) contributed to 37 sets of CT images in the training dataset and 34 in the testing dataset.

[f] Aquilion One (Toshiba) contributed to 53 sets of CT images in the training dataset and 57 in the testing dataset.

Table S3: Pairwise Comparison Results Between Different CT Acquisition and Reconstruction Parameters

Acquisition and Reconstruction Parameter	Acquisition and Reconstruction Parameter	FDR value [a]
Pitch	Rotation time	< 0.001
Pitch	Tube voltage	0.003
Pitch	Tube current	0.071
Pitch	FOV	0.001
Pitch	Slice thickness and slice interval	< 0.001
Pitch	Reconstruction kernel	< 0.001
Pitch	Iteration level	< 0.001
Rotation time	Tube voltage	< 0.001
Rotation time	Tube current	< 0.001
Rotation time	FOV	< 0.001
Rotation time	Slice thickness and slice interval	< 0.001
Rotation time	Reconstruction kernel	< 0.001
Rotation time	Iteration level	< 0.001
Tube voltage	Tube current	0.731
Tube voltage	FOV	< 0.001
Tube voltage	Slice thickness and slice interval	< 0.001
Tube voltage	Reconstruction kernel	< 0.001
Tube voltage	Iteration level	< 0.001
Tube current	FOV	< 0.001
Tube current	Slice thickness and slice interval	< 0.001
Tube current	Reconstruction kernel	< 0.001
Tube current	Iteration level	< 0.001
FOV	Slice thickness and slice interval	0.020
FOV	Reconstruction kernel	< 0.001
FOV	Iteration level	< 0.001
Slice thickness and slice interval	Reconstruction kernel	< 0.001
Slice thickness and slice interval	Iteration level	< 0.001
Reconstruction kernel	Iteration level	< 0.001

Note.—FOV = field of view. FDR = false discovery rate.

[a] Wilcoxon signed-rank test was employed and the results were corrected with the FDR method.

Table S4: The Spearman's Rank Correlation Test Results Between Each Pair of Influencing Factors [a]

Influencing Factors	Test-retest	Inter-CT	Pitch (Intra-CT protocol)	Rotation Time (Intra-CT protocol)	Tube Voltage (Intra-CT protocol)	Tube Current (Intra-CT protocol)	FOV (Intra-CT protocol)	Slice Thickness and Slice Interval (Intra-CT protocol)	Reconstruction Kernel (Intra-CT protocol)	Iteration Level (Intra-CT protocol)
Test-retest	< 0.001	< 0.001	< 0.001	< 0.001	< 0.001	< 0.001	< 0.001	< 0.001	< 0.001	< 0.001
Inter-CT	< 0.001	< 0.001	< 0.001	< 0.001	< 0.001	< 0.001	< 0.001	< 0.001	< 0.001	< 0.001
Pitch (Intra-CT protocol)	< 0.001	< 0.001	< 0.001	< 0.001	< 0.001	< 0.001	< 0.001	< 0.001	< 0.001	< 0.001
Rotation time (Intra-CT protocol)	< 0.001	< 0.001	< 0.001	< 0.001	< 0.001	< 0.001	< 0.001	< 0.001	< 0.001	< 0.001
Tube voltage (Intra-CT protocol)	< 0.001	< 0.001	< 0.001	< 0.001	< 0.001	< 0.001	< 0.001	< 0.001	< 0.001	< 0.001
Tube current (Intra-CT protocol)	< 0.001	< 0.001	< 0.001	< 0.001	< 0.001	< 0.001	< 0.001	< 0.001	< 0.001	< 0.001
FOV (Intra-CT protocol)	< 0.001	< 0.001	< 0.001	< 0.001	< 0.001	< 0.001	< 0.001	< 0.001	< 0.001	< 0.001
Slice thickness and slice interval (Intra-CT protocol)	< 0.001	< 0.001	< 0.001	< 0.001	< 0.001	< 0.001	< 0.001	< 0.001	< 0.001	< 0.001
Reconstruction kernel (Intra-CT protocol)	< 0.001	< 0.001	< 0.001	< 0.001	< 0.001	< 0.001	< 0.001	< 0.001	< 0.001	< 0.001
Iteration level (Intra-CT protocol)	< 0.001	< 0.001	< 0.001	< 0.001	< 0.001	< 0.001	< 0.001	< 0.001	< 0.001	< 0.001

Note.—FOV = field of view. FDR = false discovery rate.

[a] The results were corrected with the FDR method.

Table S5: Robustness Measurement Results of 19 Representative RFs

Trial	Test-retest	Test-retest	Inter-CT	Pitch (Intra-CT protocol)	Rotation Time (Intra-CT protocol)	Tube Voltage (Intra-CT protocol)	Tube Current (Intra-CT protocol)	FOV (Intra-CT protocol)	Slice Thickness and Slice Interval (Intra-CT protocol)	Reconstruction Kernel (Intra-CT protocol)	Iteration Level (Intra-CT protocol)	Filter
Measurement	CCC	DR	ICC	ICC	ICC	ICC	ICC	ICC	ICC	ICC	ICC	
Energy	0.989	0.970	0.989	0.989	0.992	0.990	0.989	0.904	0.984	1.000	1.000	Original
Mean	1.000	0.994	0.996	1.000	1.000	0.999	1.000	1.000	0.993	1.000	1.000	Original
wavelet.LLH_original_firstorder_90Percentile	0.939	0.908	0.922	0.919	0.941	0.939	0.940	0.929	0.940	0.970	0.953	Wavelet-LLH
wavelet.LLH_original_firstorder_Range	0.929	0.906	0.930	0.932	0.937	0.968	0.958	0.936	0.930	0.964	0.970	Wavelet-LLH
wavelet.LLL_original_firstorder_RootMeanSquared	0.999	0.990	0.994	1.000	0.999	0.999	1.000	0.999	0.999	1.000	1.000	Wavelet-LLL
square_original_firstorder_Energy	0.899	0.933	0.794	0.950	0.987	0.881	0.969	0.906	0.970	0.988	0.998	Square
square_original_firstorder_Median	0.957	0.948	0.898	0.992	0.998	0.972	0.994	0.993	0.997	0.998	0.999	Square
square_original_gldm_GrayLevelNonUniformity	0.979	0.959	0.925	0.989	0.995	0.981	0.974	0.898	0.966	0.762	0.976	Square
square_original_gldm_LargeDependenceLowGrayLevelEmphasis	0.989	0.973	0.922	0.999	0.998	0.999	0.999	0.993	0.993	0.765	0.999	Square
square_original_glrlm_LongRunLowGrayLevelEmphasis	0.915	0.948	0.810	0.982	0.992	0.982	0.993	0.901	0.982	0.886	0.989	Square
squareroot_original_firstorder_Energy	0.949	0.940	0.865	0.973	0.992	0.912	0.976	0.868	0.976	0.995	0.999	Square root
squareroot_original_glrlm_GrayLevelNonUniformity	0.953	0.933	0.887	0.932	0.967	0.822	0.889	0.867	0.931	0.845	0.865	Square root
logarithm_original_firstorder_Entropy	0.972	0.937	0.887	0.965	0.980	0.926	0.964	0.984	0.949	0.788	0.917	Logarithm
logarithm_original_glcm_Imc2	0.919	0.909	0.846	0.952	0.962	0.878	0.944	0.970	0.950	0.804	0.921	Logarithm
exponential_original_firstorder_Maximum	0.960	0.954	0.917	0.935	0.888	0.937	0.942	0.921	0.855	0.809	0.981	Exponential
exponential_original_firstorder_Minimum	0.936	0.938	0.908	0.974	0.971	0.990	0.975	0.991	0.874	0.960	0.982	Exponential
exponential_original_glrlm_RunEntropy	0.980	0.961	0.981	0.978	0.974	0.970	0.984	0.804	0.972	1.000	1.000	Exponential
exponential_original_glrlm_RunLengthNonUniformityNormalized	0.978	0.956	0.978	0.977	0.972	0.964	0.979	0.781	0.970	1.000	1.000	Exponential
lbp.2D_original_firstorder_Energy	0.939	0.903	0.913	0.940	0.967	0.947	0.945	0.795	0.892	0.784	0.992	Local binary pattern

Note.—RF = radiomic feature. FOV = field of view. CCC = concordance correlation coefficient. DR = dynamic range. ICC = intraclass correlation coefficient.

Table S6: Differential Analysis Results (FDR Values [a]) of 19 Representative RFs in Pathological Diagnosis and Semantic Features

	Pathological Diagnosis	Type of Nodule	Spiculation	Lobulation	Bubblelike Appearance	Tumor-lung Interface	Air Bronchogram	Pulmonary Vascular Change	Pleural Indentation
Energy	0.038	0.231	0.523	0.354	0.117	0.052	0.986	0.123	0.359
Mean	< 0.001	< 0.001	0.010	0.004	0.284	0.734	0.019	0.012	0.002
wavelet.LLH_original_firstorder_90Percentile	0.033	< 0.001	0.220	0.900	0.257	0.234	0.064	0.085	0.374
wavelet.LLH_original_firstorder_Range	< 0.001	< 0.001	0.112	0.161	0.179	0.017	0.010	0.012	0.667
wavelet.LLL_original_firstorder_RootMeanSquared	< 0.001	< 0.001	0.025	0.008	0.305	0.726	0.050	0.010	0.003
square_original_firstorder_Energy	0.496	0.700	0.019	0.711	0.170	0.025	0.269	0.706	0.737
square_original_firstorder_Median	0.001	< 0.001	0.001	0.025	0.008	0.222	0.082	0.011	0.063
square_original_gldm_GrayLevelNonUniformity	< 0.001	0.070	0.016	0.019	0.005	0.711	0.411	0.024	0.085
square_original_gldm_LargeDependenceLowGrayLevelEmphasis	< 0.001	< 0.001	< 0.001	0.006	0.008	0.185	0.052	0.054	0.031
square_original_glrlm_LongRunLowGrayLevelEmphasis	< 0.001	< 0.001	< 0.001	0.010	0.006	0.247	0.055	0.122	0.027
squareroot_original_firstorder_Energy	0.018	0.354	0.136	0.038	0.005	0.371	0.354	0.054	0.201
squareroot_original_glrlm_GrayLevelNonUniformity	0.494	0.206	0.024	0.829	0.354	0.112	0.234	0.442	0.746
logarithm_original_firstorder_Entropy	< 0.001	< 0.001	< 0.001	0.005	0.007	0.838	0.006	0.013	0.017
logarithm_original_glcm_Imc2	< 0.001	< 0.001	< 0.001	0.010	0.030	0.354	0.007	0.185	0.095
exponential_original_firstorder_Maximum	< 0.001	< 0.001	0.001	0.002	0.106	0.354	0.007	0.010	0.011
exponential_original_firstorder_Minimum	0.168	0.063	0.144	0.668	0.095	0.112	0.368	0.220	0.672
exponential_original_glrlm_RunEntropy	< 0.001	0.001	0.706	0.055	0.062	0.616	0.668	0.029	0.002
exponential_original_glrlm_RunLengthNonUniformityNormalized	< 0.001	0.007	0.916	0.084	0.066	0.916	0.838	0.055	0.005
lbp.2D_original_firstorder_Energy	< 0.001	0.010	0.900	0.117	0.097	0.017	0.253	0.010	0.011

Note.—FDR = false discovery rate. RF = radiomic feature.

[a] Wilcoxon rank-sum test was employed and the results were corrected with the FDR method.

Table S7: Differential Analysis Results (AUC with 95% CI) of 19 Representative RFs in Pathological Diagnosis and Semantic Features

	Pathological Diagnosis	Type of Nodule	Spiculation	Lobulation	Bubblelike Appearance	Tumor-lung Interface	Air Bronchogram	Pulmonary Vascular Change	Pleural Indentation
Energy	0.579 (0.517–0.640)	0.543 (0.483–0.604)	0.522 (0.464–0.580)	0.532 (0.471–0.594)	0.567 (0.495–0.639)	0.578 (0.506–0.650)	0.501 (0.441–0.560)	0.562 (0.491–0.632)	0.537 (0.471–0.604)
Mean	0.720 (0.662–0.778)	0.845 (0.801–0.889)	0.587 (0.530–0.644)	0.603 (0.545–0.662)	0.546 (0.474–0.618)	0.514 (0.445–0.583)	0.581 (0.524–0.639)	0.601 (0.531–0.670)	0.626 (0.558–0.695)
wavelet.LLH_original_firstorder_90Percentile	0.581 (0.516–0.645)	0.632 (0.571–0.692)	0.542 (0.484–0.599)	0.505 (0.443–0.567)	0.549 (0.474–0.623)	0.548 (0.477–0.618)	0.564 (0.506–0.623)	0.569 (0.498–0.640)	0.536 (0.470–0.602)
wavelet.LLH_original_firstorder_Range	0.636 (0.576–0.696)	0.627 (0.570–0.684)	0.553 (0.496–0.611)	0.549 (0.487–0.611)	0.558 (0.486–0.630)	0.595 (0.526–0.665)	0.591 (0.534–0.648)	0.600 (0.528–0.673)	0.519 (0.453–0.586)
wavelet.LLL_original_firstorder_RootMeanSquared	0.722 (0.664–0.780)	0.834 (0.789–0.88)	0.575 (0.518–0.632)	0.593 (0.534–0.652)	0.544 (0.473–0.616)	0.514 (0.446–0.583)	0.569 (0.511–0.627)	0.604 (0.534–0.673)	0.624 (0.555–0.693)
square_original_firstorder_Energy	0.526 (0.460–0.593)	0.515 (0.455–0.575)	0.578 (0.521–0.635)	0.487 (0.426–0.547)	0.559 (0.479–0.639)	0.589 (0.519–0.660)	0.539 (0.479–0.598)	0.516 (0.445–0.587)	0.514 (0.444–0.584)
square_original_firstorder_Median	0.622 (0.559–0.685)	0.656 (0.598–0.713)	0.613 (0.557–0.669)	0.578 (0.519–0.637)	0.616 (0.541–0.690)	0.549 (0.480–0.617)	0.561 (0.502–0.619)	0.602 (0.530–0.673)	0.576 (0.506–0.645)
square_original_gldm_GrayLevelNonUniformity	0.644 (0.584–0.704)	0.565 (0.504–0.625)	0.581 (0.524–0.638)	0.582 (0.522–0.641)	0.623 (0.550–0.697)	0.515 (0.446–0.585)	0.529 (0.469–0.588)	0.591 (0.518–0.663)	0.570 (0.502–0.639)
square_original_gldm_LargeDependenceLowGrayLevelEmphasis	0.658 (0.595–0.721)	0.725 (0.671–0.778)	0.626 (0.570–0.682)	0.598 (0.540–0.656)	0.615 (0.540–0.690)	0.553 (0.482–0.624)	0.568 (0.510–0.627)	0.577 (0.504–0.651)	0.588 (0.519–0.657)
square_original_glrlm_LongRunLowGrayLevelEmphasis	0.649 (0.586–0.712)	0.718 (0.664–0.772)	0.626 (0.570–0.682)	0.590 (0.532–0.649)	0.619 (0.546–0.693)	0.546 (0.475–0.618)	0.567 (0.508–0.626)	0.562 (0.490–0.633)	0.590 (0.523–0.657)
squareroot_original_firstorder_Energy	0.590 (0.529–0.651)	0.533 (0.473–0.594)	0.550 (0.492–0.608)	0.572 (0.512–0.633)	0.623 (0.551–0.696)	0.535 (0.466–0.605)	0.533 (0.473–0.592)	0.578 (0.505–0.650)	0.553 (0.486–0.619)
squareroot_original_glrlm_GrayLevelNonUniformity	0.527 (0.463–0.591)	0.546 (0.485–0.606)	0.576 (0.519–0.633)	0.508 (0.448–0.568)	0.540 (0.461–0.619)	0.563 (0.492–0.635)	0.542 (0.482–0.601)	0.531 (0.460–0.603)	0.513 (0.445–0.581)
logarithm_original_firstorder_Entropy	0.659 (0.598–0.719)	0.713 (0.659–0.767)	0.631 (0.575–0.686)	0.601 (0.542–0.659)	0.617 (0.542–0.691)	0.508 (0.440–0.577)	0.598 (0.540–0.655)	0.599 (0.527–0.671)	0.597 (0.530–0.665)
logarithm_original_glcm_Imc2	0.633 (0.571–0.695)	0.727 (0.675–0.779)	0.626 (0.571–0.682)	0.591 (0.531–0.651)	0.592 (0.515–0.670)	0.537 (0.465–0.610)	0.595 (0.538–0.653)	0.553 (0.482–0.625)	0.568 (0.502–0.635)
exponential_original_firstorder_Maximum	0.699 (0.642–0.757)	0.798 (0.748–0.847)	0.615 (0.559–0.671)	0.608 (0.550–0.666)	0.569 (0.500–0.638)	0.537 (0.466–0.609)	0.596 (0.538–0.653)	0.604 (0.533–0.675)	0.604 (0.536–0.673)
exponential_original_firstorder_Minimum	0.553 (0.484–0.622)	0.566 (0.505–0.628)	0.549 (0.491–0.607)	0.484 (0.424–0.544)	0.572 (0.492–0.651)	0.563 (0.495–0.632)	0.531 (0.471–0.591)	0.550 (0.479–0.620)	0.519 (0.446–0.591)
exponential_original_glrlm_RunEntropy	0.676 (0.618–0.735)	0.619 (0.560–0.678)	0.513 (0.455–0.572)	0.567 (0.506–0.628)	0.580 (0.507–0.653)	0.521 (0.447–0.596)	0.516 (0.457–0.575)	0.587 (0.518–0.657)	0.625 (0.558–0.693)
exponential_original_glrlm_RunLengthNonUniformityNormalized	0.643 (0.581–0.705)	0.598 (0.538–0.658)	0.503 (0.445–0.562)	0.560 (0.500–0.621)	0.578 (0.505–0.651)	0.496 (0.421–0.571)	0.507 (0.448–0.567)	0.577 (0.508–0.646)	0.616 (0.549–0.683)
lbp.2D_original_firstorder_Energy	0.688 (0.634–0.743)	0.594 (0.535–0.652)	0.496 (0.437–0.554)	0.555 (0.493–0.616)	0.571 (0.502–0.640)	0.595 (0.525–0.666)	0.54 (0.482–0.598)	0.605 (0.533–0.678)	0.603 (0.537–0.670)

Note.—AUC = area under curve. CI = confidence interval. RF = radiomic feature.

Table S8: The "Unstable Model" made from 1171 Unstable RFs

	Coefficient [a]	OR (95%CI)	*p* value
(Intercept)	-2.058 ± 10.664		0.847
Dependence.Entropy.(DE)	-0.040 ± 2.496	0.961 (0.007–123.826)	0.987
Small.Dependence.Low.Gray.Level.Emphasis.(SDLGLE)	-273.153 ± 128.240	0.000 (0.000–0.000)	0.033
wavelet.HLL_original_glcm_ClusterShade	-0.002 ± 0.001	0.998 (0.995–1.000)	0.127
wavelet.HHH_original_glrlm_LongRunHighGrayLevelEmphasis	-0.030 ± 0.011	0.970 (0.947–0.989)	0.007
wavelet.LLL_original_glcm_DifferenceVariance	-0.021 ± 0.019	0.980 (0.942–1.016)	0.281
square_original_glcm_ClusterShade	0.011 ± 0.005	1.011 (1.001–1.022)	0.039
squareroot_original_glcm_JointEntropy	0.847 ± 0.494	2.333 (0.941–6.598)	0.086
gradient_original_glcm_ClusterShade	0.002 ± 0.005	1.002 (0.993–1.014)	0.625
gradient_original_gldm_DependenceEntropy	-0.648 ± 3.215	0.523 (0.001–308.705)	0.840
gradient_original_gldm_GrayLevelVariance	0.220 ± 0.215	1.246 (0.822–1.931)	0.307

Note.—RF = radiomic feature. OR = odds ratio. CI = confidence interval.

[a] Plus-minus values were mean ± SD.

Table S9: The "Stable Model" made of 19 Representative RFs

	Coefficient [a]	OR (95%CI)	*p* value
(Intercept)	1.655 ± 19.277		0.932
Energy	0.000 ± 0.000	1.000 (1.000–1.000)	0.447
Mean	0.053 ± 0.049	1.055 (0.962–1.167)	0.271
wavelet.LLH_original_firstorder_90Percentile	-0.023 ± 0.010	0.977 (0.957–0.994)	0.015
wavelet.LLH_original_firstorder_Range	0.003 ± 0.001	1.003 (1.001–1.005)	0.004
wavelet.LLL_original_firstorder_RootMeanSquared	0.014 ± 0.018	1.014 (0.981–1.052)	0.435
square_original_firstorder_Energy	0.000 ± 0.000	1.000 (1.000–1.000)	0.013
square_original_firstorder_Median	-0.013 ± 0.017	0.987 (0.953–1.019)	0.459
square_original_gldm_GrayLevelNonUniformity	0.004 ± 0.014	1.005 (0.978–1.035)	0.747
square_original_gldm_LargeDependenceLowGrayLevelEmphasis	-0.020 ± 0.020	0.980 (0.940–1.020)	0.324
square_original_glrlm_LongRunLowGrayLevelEmphasis	0.157 ± 0.358	1.169 (0.535–2.462)	0.662
squareroot_original_firstorder_Energy	0.000 ± 0.000	1.000 (1.000–1.000)	0.776
squareroot_original_glrlm_GrayLevelNonUniformity	-0.251 ± 0.115	0.778 (0.615–0.965)	0.029
logarithm_original_firstorder_Entropy	-1.854 ± 2.533	0.157 (0.002–24.557)	0.464
logarithm_original_glcm_Imc2	-7.744 ± 5.950	0.000 (0.000–32.611)	0.193
exponential_original_firstorder_Maximum	0.560 ± 0.649	1.750 (0.562–7.097)	0.389
exponential_original_firstorder_Minimum	7.456 ± 9.107	1730.994 (0.000–6.835×10^{10})	0.413
exponential_original_glrlm_RunEntropy	5.938 ± 3.533	379.304 (0.450–6.006×10^{5})	0.093
exponential_original_glrlm_RunLengthNonUniformityNormalized	26.199 ± 16.500	2.388×10^{11} ($0.002–1.441\times10^{26}$)	0.112
lbp.2D_original_firstorder_Energy	0.000 ± 0.000	1.000 (1.000–1.000)	0.818

Note.—RF = radiomic feature. OR = odds ratio. CI = confidence interval.

[a] Plus-minus values were mean ± SD.